Available online at www.sciencedirect.com
ScienceDirect
Surface Science xxx (2007) xxx–xxx
SURFACE SCIENCE
www.elsevier.com/locate/susc

Facet-edge fluctuations with periphery diffusion kinetics

M. Degawa [a], T.J. Stasevich [a], A. Pimpinelli [b], T.L. Einstein [a], E.D. Williams [a,*]

[a] Department of Physics, Materials Research Science and Engineering Center, University of Maryland, College Park, MD 20742-4111, USA
[b] LASMEA, UMR 6602 CNRS, Université Blaise Pascal, Clermont 2, F-63177 Aubière Cedex, France

Abstract

We investigate the novel scaling of the steps bounding a facet surrounded by a rough region. The hindered, asymmetric fluctuations can be associated with the emergence of a dominant non-linear term in the Hamiltonian governing the step fluctuations. We explore the crossover from unhindered to hindered fluctuations, calculating the growth exponent, β, with Monte Carlo simulation within the TSK model. The hindered behavior is found in the simulations when the facet-edge step is separated by fewer than six atomic spacings from the second step. Actual fluctuations are larger than in this calculation, particularly at higher temperatures, making the hindered behavior easier to observe. In addition, we discuss the possibility that volume conservation effects in nanoscale structures may cause similar confinement in non-conserved fluctuations.

Keywords: Equilibrium thermodynamics and statistical mechanics; Terrace-step-kink model; Monte Carlo simulations; Surface diffusion; Surface (step) tension; Kinks; Steps; Adatoms

1. Introduction

Due to the rapid growth of interest in quantum computing and the related demand for creating quantum dots, controlled fabrication of nano-structures has become of great importance [1–4]. For the evolution of nano-structure, the control of step dynamics is crucial, since the steps are the fundamental building blocks of crystalline surfaces. The equations of motion for straight steps on a vicinal surface are well understood within the continuum step model e.g. as applied to MBE growth and step bunching. The power of this model is that it can be applied to both analysis of experimental observations [5–8] and comparison to microscopic models, such as the terrace-step-kink (TSK) model, using statistical methods and a handful of key parameters [6,9]. In particular, Langevin-type analysis of the statistical properties of steps can be used to relate the physical properties of isolated steps to the thermodynamic parameters of the continuum step model. Application of the Langevin approach has shown that the experimentally accessible correlation functions (defined below) scale as $\sim y^{2\alpha}$ and $t^{2\beta}$, where α and β are the roughness and growth exponents, respectively. For isolated steps, $\alpha = 1/2$, characteristic of a random walk, and β depends on the principal mass transport mechanism, e.g. attachment–detachment (A/D), $\beta = 1/4$, and periphery diffusion (PD), $\beta = 1/8$ [5,6].

However, for nano-structures, the step equations of motion are not obvious due to the finite volume effects of the nano-structure [10,11]. Although the steps can still be viewed as 1D interfaces, not only local deformations but global effects (overall shape and mass conservation) must be considered to obtain the equations of motion. In a previous paper [12], we showed that a global curvature of an island or a step at a facet-edge, as illustrated in Fig. 1a and b, alters the step chemical potential compared to an isolated step by breaking the symmetry of adatom motion to the upper and lower terrace, resulting in a non-linear equation of motion for the step. For a facet, furthermore, the suppression of the fluctuation amplitude due to the existence of a neighboring step alters the scaling behavior of the noise term in the Langevin equation. Such changes lead to two different university classes of dynamic scaling,

* Corresponding author. Tel.: +1 301 405 6156; fax: +1 301 314 9465.
E-mail address: edw@physics.umd.edu (E.D. Williams).

0039-6028/$ - see front matter © 2007 Elsevier B.V. All rights reserved.
doi:10.1016/j.susc.2007.04.097

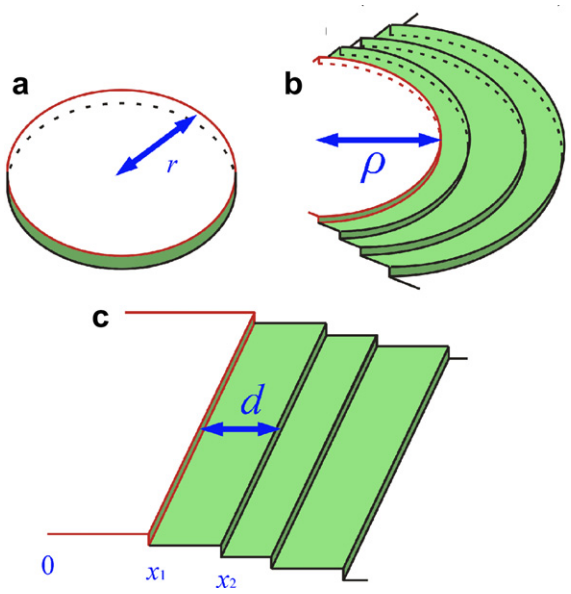

Fig. 1. Schematic drawing of the continuum step model in the three cases of (a) an island with radius r (b) a facet of a finite volume crystallite (with curvature) with radius ρ and (c) a facet of a infinite volume crystallite (straight steps) with $d = x_2 - x_1$.

with $\alpha = 1/3$ [13] for both and $\beta = 1/5$ and $\beta = 1/11$ for A/D and PD, respectively [12].

Another previous conclusion [12] was that the global curvature effect will be important for an island only when its circumference is small compared to the capillary length; this translates to a very severe condition on the equilibrium chemical potential of the island ($\mu_{eq} > 2\pi\beta\tilde{\beta}\Omega/k_BT$) [14,15]. In this paper, we show with the use of the continuum step model that even with no curvature (straight steps), a facet-edge step interacting with a single fixed neighboring step, with dynamics conserving mass, can have a non-linear term in the equation of motion. Monte Carlo simulations using the TSK model are performed to confirm the proposed effects.

2. Background

The continuum step model uses a discrete array of 1D continuous interfaces to represent the steps on the surface. A facet-edge step of a crystallite with infinite volume (straight steps) is illustrated in Fig. 1c. With appropriate approximations, the step equation of motion is given by a Langevin equation

$$\frac{\partial x(y,t)}{\partial t} = f[x(y,t)] + \eta(y,t), \tag{1}$$

where $x(y,t)$ is the position of the facet-edge at time t, $f[\bullet]$ is a function of $x(y,t)$ describing the deterministic relaxation process, and $\eta(y,t)$ is a noise term, which can be conservative or non-conservative depending on the nature of $f[\bullet]$. The free energy of the facet step with a projected length L is

$$F = \int_0^L \left(\beta(\theta)\sqrt{1 + \left(\frac{\partial x}{\partial y}\right)^2} + \frac{gh^3}{(x_2 - x)^2} \right) \mathrm{d}y, \tag{2}$$

where β is the step free energy per length, g is the step interaction coefficient, h is the step height and x_2 is the position of the neighboring step, which is approximated as straight and fixed in position. The step chemical potential is derived as

$$\mu[x,\dot{x},\ddot{x}] = \frac{\delta F}{\delta N} = \Omega\left(\frac{-\tilde{\beta}\ddot{x}}{\sqrt{(1+\dot{x}^2)^3}} + \frac{2gh^3}{(x_2 - x)^3} \right), \tag{3}$$

where Ω is the atomic area, $\tilde{\beta} = \beta + \partial^2\beta/\partial\theta^2$ is the step stiffness, and the superscript dot denotes differentiation with respect to y. The deterministic part of the Langevin equation is obtained by modeling the microscopic transfer processes at the facet step-edge. Non-conserved dynamics is used to represent the random A/D of adatoms from the reservoir as

$$\frac{\partial x(y,t)}{\partial t} = \frac{-\Gamma_{AD}}{k_BT}\mu[x,\dot{x},\ddot{x}] + \eta(y,t), \tag{4}$$

where Γ_{AD} is the A/D-driven step mobility and $\eta(y,t)$ is non-conserved white noise. Similarly for PD, conserved dynamics is used to represent atoms moving along the step edge

$$\frac{\partial x(y,t)}{\partial t} = \frac{\Gamma_{PD}}{k_BT}\frac{\partial^2 \mu[x,\dot{x},\ddot{x}]}{\partial y^2} + \eta_C(y,t), \tag{5}$$

where Γ_{PD} is the edge-hopping-driven step mobility (differing from Γ_h of Ref. [5] by a factor of Ω), and $\eta_C(y,t)$ is conserved white noise.

3. Results

To obtain the stable mean position x_1 of the facet-edge, Eq. (3) is set equal to the "reservoir" chemical potential μ_0 of the crystallite [11]. Neglecting the local curvature term (first term) in Eq. (3) gives

$$x_1 = x_2 - h\left(\frac{2\Omega g}{\mu_0}\right)^{1/3} \quad \text{or} \quad d = h\left(\frac{2\Omega g}{\mu_0}\right)^{1/3} \tag{6}$$

where $d = x_2 - x_1$ is the distance between the top two steps as shown in Fig. 1c. Assuming the fluctuations to be small, Eq. (3) is expanded about this x_1.

$$\mu[x,\ddot{x}] = -\Omega\tilde{\beta}\ddot{x} + \mu_0 + \frac{3}{h}\left(\frac{\mu_0^4}{2\Omega g}\right)^{\frac{1}{3}}(x - x_1) + \frac{3}{h^2}\left(\frac{2\mu_0^5}{\Omega^2 g^2}\right)^{\frac{1}{3}}(x - x_1)^2 + \cdots. \tag{7a}$$

Using dimensionless variables,

$$\tilde{x} = \frac{x - x_1}{d}, \quad \tilde{y} = \frac{y}{d}, \quad \tilde{\mu} = \frac{\mu d}{\Omega\tilde{\beta}}, \quad \tilde{g} = \frac{gh^3}{\tilde{\beta}d^2} \tag{7b}$$

we obtain:

$$\tilde{\mu}[\tilde{x},\dot{\tilde{x}}] = -\ddot{\tilde{x}} + 2\tilde{g} + 6\tilde{g}\tilde{x} + 12\tilde{g}\tilde{x}^2 + \cdots. \tag{7c}$$

Thus, with $\tilde{t} = (\Gamma_{\mathrm{PD}}\Omega\tilde{\beta}/k_{\mathrm{B}}Td^4)t$, the dimensionless Langevin equation in the PD case is

$$\frac{\partial\tilde{x}(y,t)}{\partial\tilde{t}} = -\frac{\partial^4\tilde{x}}{\partial\tilde{y}^4} + 2\tilde{g} + 6\tilde{g}\frac{\partial^2\tilde{x}}{\partial\tilde{y}^2} + 24\tilde{g}\left(\frac{\partial\tilde{x}}{\partial\tilde{y}}\right)^2 + \cdots + \tilde{\eta}_{\mathrm{C}}(y,t) \tag{8}$$

where $\tilde{\eta}_C = (\Gamma\Omega\tilde{\beta}/k_{\mathrm{B}}Td^3)\eta_{\mathrm{C}}$. All higher order terms in $\tilde{x}$ are negligible since $\tilde{x} \ll 1$. The fourth term on the right hand side of Eq. (8) is non-linear, characteristic of the Kardar–Parisi–Zhang (KPZ) equation, and has the same form as the non-linear term that arises from the global curvature effect [12]. If dominant, such a non-linear term can lead to totally different behavior in the shape evolution of nanocrystallites. The dominance at the short and long times is determined by the relative magnitude of the coefficients of each term. The physical origin here, however, arises from the asymmetry of the effective potential which the facet step experiences from the fixed single neighboring step, which also breaks the symmetry of adatom motion to the lower and upper terrace. The effective potential (grand potential) $\Xi(x)$ is obtained from the free energy in Eq. (2) and the "reservoir" chemical potential μ_0

$$\tilde{\Xi}(\tilde{x}) = \frac{\beta}{\tilde{\beta}} + \frac{\tilde{g}}{(1-\tilde{x})^2} - 2\tilde{g}(\tilde{x}+\tilde{x}_1), \cong \text{const.} + 3\tilde{g}\tilde{x}^2 + 4\tilde{g}\tilde{x}^3 + \cdots, \tag{9}$$

where $\tilde{\Xi}(\tilde{x}) = \Xi(x)/\tilde{\beta}L, \tilde{x}_1 = x_1/d$. Note that when $\tilde{g} = 0$, Eq. (9) is a constant, and Eq. (8) reduces to the equation of motion for an isolated straight step.

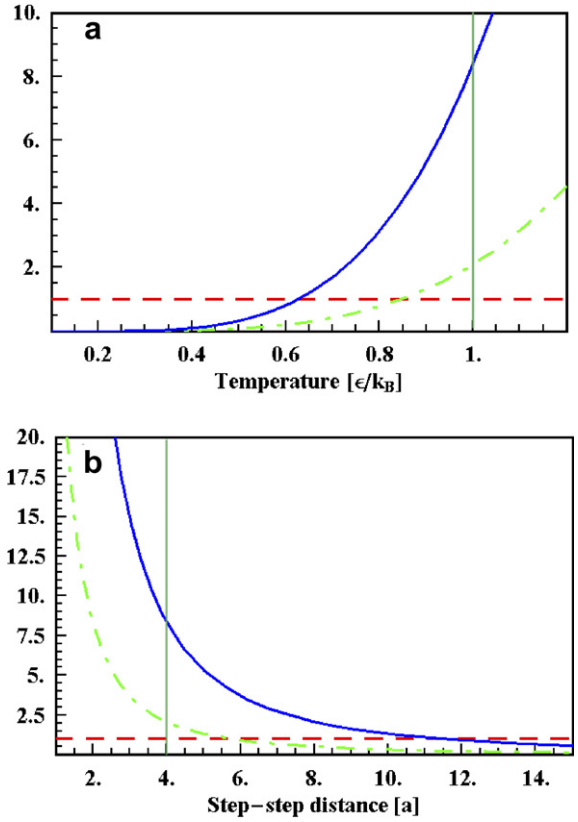

Fig. 2. Magnitude of the three coefficients in Eq. (8) as a function of (a) temperature $T[\varepsilon/k_{\mathrm{B}}](d=4)$ and (b) step–step distance $d[a](T=1)$. The fourth-order derivative term, second-order derivative term, and the non-linear KPZ term are given as a dashed, dash–dot and solid line, respectively. The thermodynamic parameters, step free energy β, step stiffness $\tilde{\beta}$ and step–step interaction coefficient g, were calculated with the TSK model. The thin vertical line is $T=1$ and $d=4$ in (a) and (b), respectively.

4. Simulation

Metropolis Monte Carlo (MC) simulations, valid for equilibrium, were performed based on a standard TSK model (square lattice with steps along a close-packed direction) with PD kinetics. In the TSK model the only excitations are thermal kinks with energy ε along a step described by a single-valued function $x_n(y)$, where n is the step number. The term $\varepsilon|x_n(y+1) - x_n(y)|$ in the Hamiltonian leads to a step free energy per unit length of $\beta = \varepsilon/a + (k_{\mathrm{B}}T/a)\ln[\tanh(\varepsilon/2k_{\mathrm{B}}T)]$ [16] (a, atomic length) and step stiffness of $\tilde{\beta} = (2k_{\mathrm{B}}T/a)\sinh^2(\varepsilon/2k_{\mathrm{B}}T)$ [17]. The non-touching constraint $x_{n+1}(y) > x_n(y)$ results in an entropic repulsion gh^3/l^2, where l is the step–step distance and $g = (\pi k_{\mathrm{B}}T)^2/6h^3\beta$ [18]. PD kinetics is obtained by moving atoms to their neighboring sites from randomly chosen step positions. For an atom to move, it must break and reform bonds; if there are just nearest neighbor bonds, the net change in energy has only three possibilities, corresponding to the net gain/loss of 2 ($\pm 4\varepsilon$), 1 ($\pm 2\varepsilon$), or 0 bonds.

From the results above, the magnitude of the coefficients of each term in Eq. (8) can be calculated within the TSK model and are given in Fig. 2 as a function of (a) temperature T (in units $\varepsilon/k_{\mathrm{B}}$) with $d=4$ (in units of a) and (b) step–step distance d with $T=1$. The fourth-order derivative term, second-order derivative term and the non-linear KPZ term are shown as dashed, dash–dot and solid lines, respectively. At high temperatures and small step–step distance, the KPZ term should dominate at long time. For large step–step distances the fourth-order derivative term is always dominant, a situation equivalent to an isolated step. Note that the TSK model underestimates fluctuations at high temperatures since overhangs are prohibited; the Ising model is more appropriate [19]. Fortunately, similar calculations of the step free energy using the Ising model [20] show that qualitative features of the TSK model are still valid although the curves equivalent to those in Fig. 2 will differ quantitatively at high temperature. For calibration, note that $\tilde{\beta}_{\mathrm{TSK}}/\tilde{\beta}_{\mathrm{Ising}}$ is $\sim$1.2 at $T=0.8$ and $\sim$2.4 at $T=1$. We used the relatively high temperature in order to achieve adequate statistics in our simulations in our limited runs.

For statistical analysis of facet step-edge fluctuations, we calculated the spatial and time correlation functions, $G(y,t_0)$ and $G(y_0,t)$, respectively,

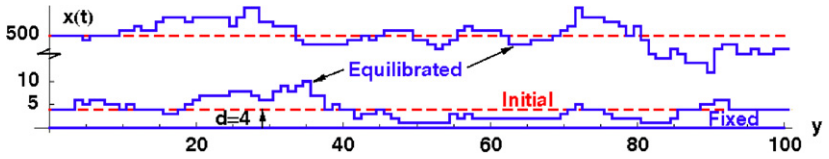

Fig. 3. A snap shot of the MC configuration, $x(y)$ of an isolated step ($d = 500$) and $d = 4$ for $T = \varepsilon/k_B$ and $L = 100$. Initial step and equilibrated step are shown as dashed and solid line, respectively. The $x = 0$ line is the position of the fixed neighboring step.

$$G(y, t_0) = \left\langle [x(y + y_0, t_0) - x(y_0, t_0)]^2 \right\rangle_{y_0}, \quad (10a)$$

$$G(y_0, t) = \left\langle [x(y_0, t + t_0) - x(y_0, t_0)]^2 \right\rangle_{t_0}, \quad (10b)$$

for a fully equilibrated step (i.e.after the width has attained its saturation value).For lengths and times shorter than the correlation length and crossover time, the correlation functions scale as $G(y,t_0) \sim y^{2\alpha}$ and $G(y_0, t) \sim t^{2\beta}$, yielding the roughness exponent α and growth exponent β.Fig.3 shows a MC snapshot of an essentially isolated step ($d = 500$ [a]) and $d = 4$ at $T = 1$ [ε/k_B] and $L = 100$ [a], initially (dashed) and after equilibration (solid) (also see Ref.[21]).To simulate confinement, the neighboring step is fixed at distances $d = 2, 3, 4, 5, 6$ [a].Fig.4 shows $G(y_0, t)$ obtained after equilibration for 10^7 MCS (MC steps per site) and averaged over 10 realizations.Fig.4a shows results for $d = 4$.The fit to the data shows definite crossover.At early times the slope is $m \sim 0.25$ and later $m \sim 0.18$, close to the predicted values of $2\beta = 1/4$ and $2\beta = 2/11$ for isolated and facet (confined) step-edge fluctuations, respectively, with PD kinetics.Fig.4b shows results for $d = 2, 3, 4, 5, 6$ and 500.For $d = 2$ the neighboring step is so close that no type of power-law behavior can be identified.As the step–step distance increases, the crossover time from $2\beta = 1/4$ to $2\beta = 2/11$ also increases.When $d > 6$, within the range of 10^7 MCS, crossover time is not observed, and the slope shows $2\beta = 1/4$.From the results of $d = 500$ [a] we can estimate Γ_{PD}, since the result for an isolated step is analytically known [6,8,22], and obtain $\Gamma_{PD} = 0.213$ [a^3/MC steps].Using this result, an estimated crossover time $\tilde{t} = (24\tilde{g})^{-4/3}$ from $2\beta = 1/4$ to $2\beta = 2/11$ gives $t = 130$ MC steps for $d = 4$ [a], which is fairly close to the results in Fig.4a for a crude estimate forΓ_{PD}. Fig. 5 shows results of $G(y,t_0)$ obtained after equilibration for $d = 4$ [a] and $d = 500$ [a]. Since the length of the step is limited, it is difficult to say anything conclusive; however, the initial portion of the data is fit to a slope of $m \sim 0.67$ and $m \sim 1.0$ for $d = 4$ [a] and $d = 500$ [a], consistent with the prediction of $2\alpha = 2/3$ and $2\alpha = 1$ for confined and isolated steps, respectively.

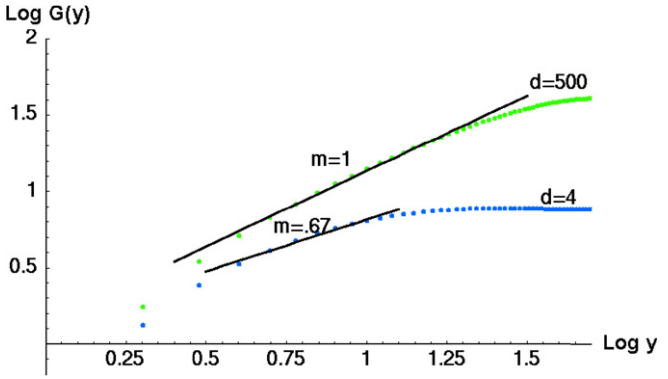

Fig. 5. Log–log plot of $G(y, t_0)$ obtained after equilibration for $d = 4$ and $d = 500$. The fit of the slope m (i.e. 2α) is ~0.67 and ~1 for $d = 4$ and $d = 500$, respectively.

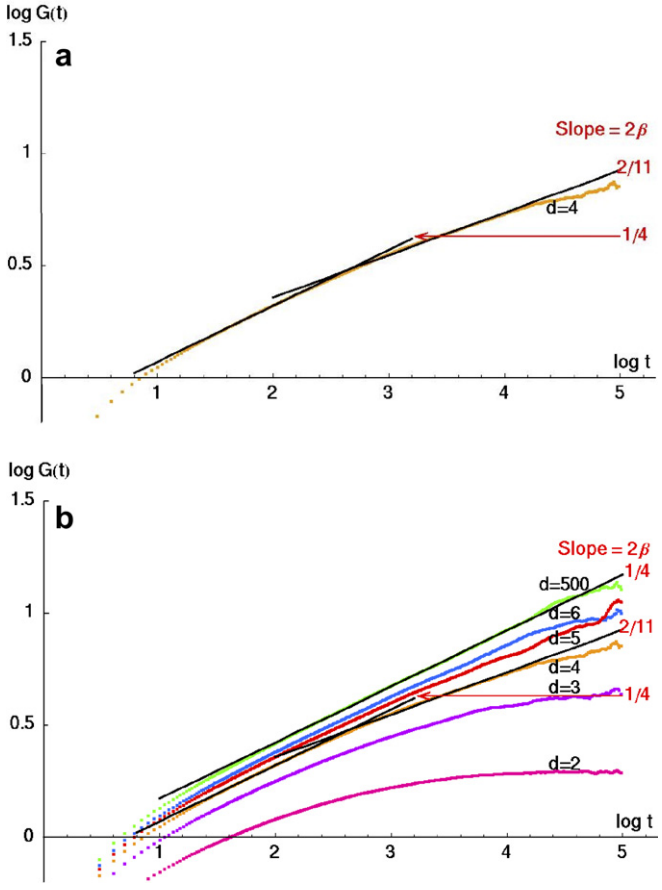

Fig. 4. Log–log plot of $G(y_0, t)$ obtained from 10^7 MC steps per site after equilibration and averaged over 10 realizations. (a) Shows results for $d = 4$ with a fit to the slope of ~0.25 and ~0.18, close to the predicted values of $2\beta = 1/4$ and $2\beta = 2/11$. (b) Shows results for $d = 2 \sim 500$. For $d = 2$ the logarithmic behavior ($\beta = 0$) is observed and for $d = 500$ it is $2\beta = 1/4$.

5. Discussion

Only for a limited range of crystallite size d is the nonlinear term dominant in the dynamics. In our TSK model, the upper end of this range is ~12 [a] (Fig. 2b), where the

scaling crosses over to isolated step behavior ($\beta = 1/8$); the lower end is ~ 3 [a] (Fig. 4b) where $\tilde{x} \ll 1$ becomes invalid, and the logarithmic ($\beta = 0$) behavior characteristic of a step in a 2D step train [5] is seen. This seems to imply an extremely limited range of conditions. The actual range for experimental observations of non-linear-dominated behavior is considerably larger than the narrow range predicted by this model. First, the TSK model greatly underestimates fluctuations at high temperatures: more realistic models allowing more complex excitations e.g. the Ising model, increase the effect of the non-linear term. Secondly, only entropic interactions are considered here. Generally there are also elastic ones, which increase the value of d (by $d \sim g^{1/2}$ for straight steps [5]) also enhancing the non-linear term effect. Third, no global curvatures are considered here, which increases the asymmetry of the effective potential in Eq. (9). Such considerations raise substantially the upper limit for d, which make experimental observations with a restricted time range more likely [21].

Although PD is known to be the dominant mass transfer process for many metal (1 1 1) surfaces at moderate temperature [5,6], A/D cannot be completely neglected in real systems, in contrast to the present simulations. Since Eqs. (4) and (7c) show that A/D does not generate the non-linear term, the experimental relevance of our results may also appear rather limited. Again, this is not the case, for a subtle reason that stems from arguments of the conservation of mass. At equilibrium, for a crystallite with fixed volume, the individual layers fluctuate, exchanging matter among themselves, not with any reservoir. Thus far from the facet, fluctuations are strongly suppressed due to high step density and volume conservation: energy barriers quash mass transfer. The net result is that adatoms detaching from the facet-edge have a strong tendency to return, as for step fluctuations in the presence of a strong Ehrlich-Schwoebel barrier [22], and so one finds the same dynamical exponents as PD [22]. Thus, it may be possible to see qualitatively similar effects for confined step fluctuations even when mass transport includes other physical mechanisms.

However, there is a more serious contradiction between simulation and theory. We observe $\beta = 1/11$ in the simulation, which is characteristic of PD with global curvature [12] and not characteristic for the KPZ term with conserved noise, although they are both non-linear terms. This may suggest a possible step-step interaction in the simulation depending on local angle; this scenario is beyond the scope of the present work and will be the subject of future investigation.

Acknowledgements

Work at University of Maryland has been supported by the UMD-NSF MRSEC under Grant DMR 05-20471; visits by A.P. supported by a CNRS Travel Grant. The shared experimental facilities of the MRSEC were used in the related experimental work.

References

[1] I. Lyubinetsky, S. Thevuthasan, D.E. McCready, D.R. Baer, Journal of Applied Physics 94 (2003) 7926.
[2] Z. Gai, B. Wu, J.P. Pierce, G.A. Farnan, D.J. Shu, M. Wang, Z.Y. Zhang, J. Shen, Physical Review Letters 89 (2002) 235502.
[3] J. Tersoff, C. Teichert, M.G. Lagally, Physical Review Letters 76 (1996) 1675.
[4] C. Teichert, M.G. Lagally, L.J. Peticolas, J.C. Bean, J. Tersoff, Physical Review B 53 (1996) 16334.
[5] H.C. Jeong, E.D. Williams, Surface Science Reports 34 (1999) 175.
[6] M. Giesen, Progress in Surface Science 68 (2001) 1.
[7] I. Lyubinetsky, D.B. Dougherty, T.L. Einstein, E.D. Williams, Physical Review B 66 (2002) 085327.
[8] O. Bondarchuk, D.B. Dougherty, M. Degawa, E.D. Williams, M. Constantin, C. Dasgupta, S. Das Sarma, Physical Review B 71 (2005) 045426.
[9] T.J. Stasevich, H. Gebremariam, T.L. Einstein, M. Giesen, C. Steimer, H. Ibach, Physical Review B 71 (2005) 245414.
[10] Z. Kuntová, Z. Chvoj, V. Šíma, M.C. Tringides, Physical Review B 71 (2005) 125415.
[11] M. Degawa, F. Szalma, E.D. Williams, Surface Science 583 (2005) 126.
[12] A. Pimpinelli, M. Degawa, T.L. Einstein, E.D. Williams, Surface Science 598 (2005) L355.
[13] P.L. Ferrari, M. Prähofer, H. Spohn, Physical Review E 69 (2004) 035102.
[14] B. Krishnamachari, J. McLean, B. Cooper, J. Sethna, Physical Review B 54 (1996) 8899.
[15] K. Morgenstern, G. Rosenfeld, E. Lægsgaard, F. Besenbacher, G. Comsa, Physical Review Letters 80 (1998) 556.
[16] C. Rottman, M. Wortis, Physical Review B 24 (1981) 6274.
[17] N.C. Bartelt, T.L. Einstein, E.D. Williams, Surface Science 276 (1992) 308.
[18] Y. Akutsu, N. Akutsu, T. Yamamoto, Physical Review Letters 61 (1988) 424.
[19] N.C. Bartelt, T.L. Einstein, E.D. Williams, Surface Science 240 (1990) L591.
[20] N. Akutsu, Y. Akutsu, Surface Science 376 (1997) 92.
[21] M. Degawa, T.J. Stasevich, W.G. Cullen, A. Pimpinelli, T.L. Einstein, E.D. Williams, Physical Review Letters 97 (2006) 080601.
[22] A. Pimpinelli, J. Villain, D.E. Wolf, J.J. Métois, J.C. Heyraud, I. Elkinani, G. Uimin, Surface Science 295 (1993) 143.